High-Order Harmonic Generation and Its Unconventional Scaling Law in the Mott-Insulating Ca_2RuO_4

K. Uchida,[1,*] G. Mattoni,[1] S. Yonezawa,[1] F. Nakamura,[2] Y. Maeno,[1] and K. Tanaka[1,†]
[1]*Department of Physics, Graduate School of Science, Kyoto University, Kyoto, Kyoto 606-8502, Japan*
[2]*Department of Education and Creation Engineering, Kurume Institute of Technology, Kurume, Fukuoka 830-0052, Japan*

(Received 30 June 2021; revised 17 January 2022; accepted 10 February 2022; published 23 March 2022)

Competition and cooperation among orders is at the heart of many-body physics in strongly correlated materials and leads to their rich physical properties. It is crucial to investigate what impact many-body physics has on extreme nonlinear optical phenomena, with the possibility of controlling material properties by light. However, the effect of competing orders and electron-electron correlations on highly nonlinear optical phenomena has not yet been experimentally clarified. Here, we investigated high-order harmonic generation from the Mott-insulating phase of Ca_2RuO_4. Changing the gap energy in Ca_2RuO_4 as a function of temperature, we observed a strong enhancement of high order harmonic generation at 50 K, increasing up to several hundred times compared to room temperature. We discovered that this enhancement can be well reproduced by an empirical scaling law that depends only on the material gap energy and photon emission energy. Such a scaling law can hardly be explained by the electronic structure change in the single particle model and has not been predicted by previous theoretical studies on HHG in the simple Mott-Hubbard model. Our results suggest that the highly nonlinear optical response of strongly correlated materials is influenced by competition among the multiple degrees of freedom and electron-electron correlations.

DOI: 10.1103/PhysRevLett.128.127401

Strong coupling among multiple degrees of freedom often results in a variety of electronic ground states, especially in strongly correlated materials. A strong light field may drive such systems far from equilibrium and modify the balance among competing orders. After light irradiation, the material can relax to a non-trivial metastable state such as a transient superconducting state or a ferroelectric state [1–4]. Under a strong light field, coherent and highly nonlinear optical phenomena can also be observed. High order harmonic generation (HHG) is the most typical of such phenomena [5–15], where coherent photons with integer multiples of the driving photon energy are emitted. HHG has provided fundamental insights into nonperturbative light-matter interactions in solids [13]. So far, HHG has mainly been studied in systems that can be described with the single electron approximation, giving information about the band structure [7,8], interatomic bonding [9,14], Berry curvature [11], and transition dipole moment [15]. HHG spectroscopy is applicable to strongly correlated systems, where electron-electron correlations play a dominant role, and has the potential to be a new method to elucidate the dynamical aspects of many-body physics. Several theoretical studies predict the characteristics of HHG for strongly correlated materials [16–20]. However, only a few HHG experiments have been performed so far on strongly correlated materials [21,22], and the unique properties related to their electronic correlations has yet to be found.

In this Letter, we report HHG from the Mott-insulating phase of Ca_2RuO_4 with a strong enhancement of HHG yields upon lowering temperature. The strongly temperature-dependent gap energy of Ca_2RuO_4 allows us to investigate the relationship between HHG emission and the gap energy in this strongly correlated system. We find that the yields of the high harmonics scale with the gap energy and the high harmonic emission energy. The observed scaling law cannot be reproduced by the electronic structure change in single particle model or by previous theoretical studies about HHG in strongly correlated materials. This indicates that electron-electron correlations and the interplay of multiple degrees of freedom in Ca_2RuO_4 play a crucial role in its highly nonlinear optical response.

Ca_2RuO_4 is a layered perovskite which shows a variety of electronic properties owing to the competition between multiple degrees of freedom [23,24]. The material is a Mott insulator below the metal-insulator transition temperature $T_{MI} \sim 360$ K and shows antiferromagnetic order below $T_N \sim 110$ K [25]. The electronic properties can be

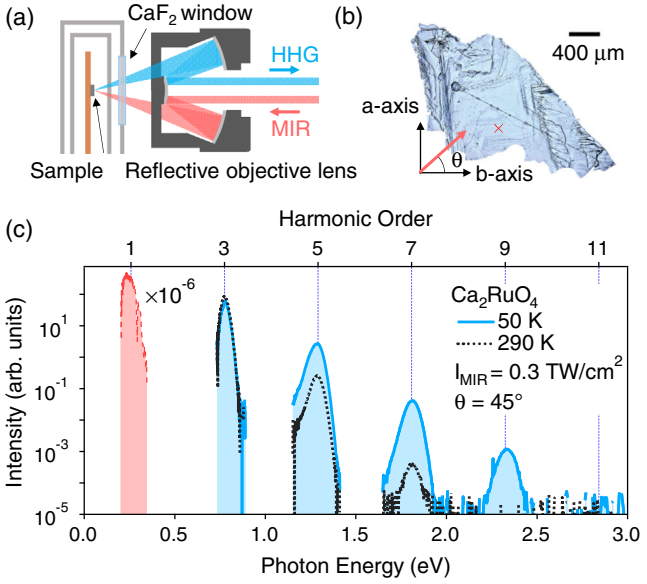

FIG. 1. High harmonic generation in Ca_2RuO_4. (a) Schematic diagram of the experimental setup for HHG measurement in reflection geometry (extended details in Fig. S3 in the Supplemental Material [30]). (b) Optical image of the Ca_2RuO_4 sample. The position of the MIR spot, that is focused on a region where the sample surface roughness is small, is indicated by the red cross mark (spot diameter 27 μm). The red arrow indicates the direction of the MIR polarization which is identified by the angle θ that it forms with the b axis. (c) Typical HHG spectra obtained at 50 (light-blue curve and shaded area) and 290 K (black dotted line) with MIR intensity of 0.3 TW/cm^2 and polarization $\theta = 45°$. The red curve and shaded area indicate the incident MIR spectrum, measured using a monochromator equipped with a HgCdTe detector, that is decreased by a factor of 10^{-6} in the plot for clarity.

controlled by varying external parameters such as chemical substitution [26], pressure [27], electric field [28], and temperature [25]. The gap energy of Ca_2RuO_4 changes from 0.2 to 0.65 eV upon lowering temperature below T_{MI} [29].

We used an intense midinfrared (MIR) pulse (central photon energy: $\hbar\Omega_{MIR} = 0.26$ eV, repetition rate: 1 kHz, and pulse duration: 100 fs) to measure HHG emissions from samples of Ca_2RuO_4. Figure 1(a) shows a schematic view of the experimental setup [30]. The sample was set in an optical cryostat, and its temperature was varied between 290 and 50 K within Ca_2RuO_4 Mott insulating phase. MIR pulses were focused onto the sample using a reflective-type objective lens and passed through a 1-mm-thick CaF_2 window. The typical MIR intensity at the focus point in vacuum is 0.3 TW/cm^2, corresponding to an electric field strength of 15 MV/cm, and pulse energy of around 0.3 μJ (spot diameter 27 μm). Since bulk Ca_2RuO_4 is not transparent above the gap energy, we collected the HHG signal in reflection geometry using the same objective lens. In this configuration, we have the advantage of a negligible nonlinear propagation effect that in other configurations would strongly distort the spectral shape [34–36]. Figure 1(b) shows an optical image of a single crystal Ca_2RuO_4 sample with an exposed ab plane. The transition temperatures ($T_{MI} = 360$ and $T_N = 110$ K) were confirmed by magnetic susceptibility measurements [30]. The crystal orientation was determined by x-ray diffraction as well as by magnetic anisotropy measurements. Throughout the experiment, we used a linearly polarized MIR pulse with polarization lying in the ab plane, and electric field direction (polarization) identified by the angle θ with respect to the b axis [Fig. 1(b)].

Figure 1(c) shows typical HHG spectra obtained at 290 K (black dotted line) and 50 K (light blue line and shaded area) with an incident MIR intensity I_{MIR} of 0.3 TW/cm^2 and $\theta = 45°$. We observed only odd-order harmonics because of the inversion symmetry of Ca_2RuO_4. While the third-order harmonic yield is just slightly suppressed at low temperature, we observe a strong enhancement of the fifth and higher harmonics. The enhancement is stronger for larger harmonic order, reaching several hundred times yield for the ninth harmonic at 50 compared to 290 K.

Changes of Ca_2RuO_4 optical properties in the MIR region can change the excitation conditions, possibly accounting for part of this enhancement. However, we estimated that the change of the MIR electric field inside the sample due to its reflectivity change between 290 and 50 K is less than 7% [30]. As it will be shown in Figs. 2(a)–2(c), this change can only explain an increase of the HHG signal of just about 25%. This fact indicates that the observed enhancement in HHG intensity has a different origin, possibly intrinsic to the nonlinearity of the material.

We now study the dependence of the nth-order harmonic intensity I_n on the incident MIR intensity I_{MIR}. There are strong deviations from the predictions of perturbative nonlinear optics ($I_n \propto I_{MIR}^n$, dotted lines in Figs. 2(a)–2(c)), because all HHG intensities are almost proportional to the square of MIR intensity ($I_n \propto I_{MIR}^2$). This indicates that nonperturbative light-matter interactions take place under our experimental conditions. Moreover, the dependences of the normalized HHG intensities on the MIR intensity are almost unchanged in the studied temperature range. These results suggest that the microscopic HHG mechanism is unaffected by changes in temperature.

Figures 2(d)–2(f) show the crystal-orientation dependence of the third, fifth, and seventh harmonic intensities at 290 and 50 K. All the harmonics show maximum values for $\theta \sim 45°$, for which the MIR electric field points along the direction from Ru to nearest-neighbor Ru or O atoms [Fig. 2(g)]. This suggests that interatomic transitions such as intersite d-d transitions or charge transfer transitions may be involved in the HHG process [9,22]. Since HHG emission energies are in the region of the d-d transition [29], the anisotropy of HHG yields may be attributed to d-d transitions between nearest-neighbor Ru ions. By lowering

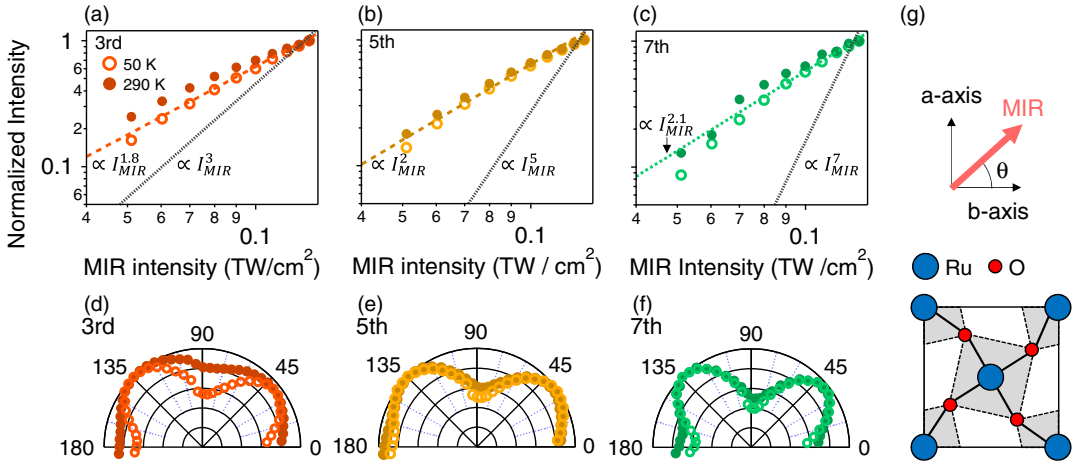

FIG. 2. Dependence of the HHG yields on MIR intensity and polarization. (a)–(c) Normalized (a) third, (b) fifth, and (c) seventh harmonic intensity as a function of MIR intensity with MIR polarization angle $\theta = 45°$. Open circles measured at 50 K, solid circles measured at 290 K. All the harmonic intensities are normalized by their peak value. Dashed lines are guides to the eye which are proportional to $I_{\mathrm{MIR}}^{1.8}$, I_{MIR}^{2}, and $I_{\mathrm{MIR}}^{2.1}$. The black dotted lines indicate the trends expected from perturbation theory ($I_n \propto I_{\mathrm{MIR}}^{n}$, n: harmonic order). (d)–(f) Polar plots of the (d) third, (e) fifth, and (f) seventh harmonic intensity as a function of MIR polarization angle θ. The MIR intensity was fixed at the maximum value of 0.3 TW/cm^2. (g) Schematic of the Ru-O plane in Ca_2RuO_4 respect to which the polarization is changed. The gray shaded areas indicate the oxygen octahedra.

the temperature, the HHG anisotropy becomes stronger. However, this increased anisotropy is not salient in the fifth and seventh harmonics, even though strong enhancements in their HHG yields are observed. These results support the fact that the HHG mechanism is not directly caused by changes in temperature.

To investigate the temperature dependence in more detail, we measured HHG intensities with $\theta = 45°$ as a function of temperature. Normalized intensities of nth-order harmonics $I_n(T)$ are shown in Figs. 3(a)–3(d) (solid circles). HHG intensities in Ca_2RuO_4 do not show any noticeable variation in proximity of the Néel transition ($T_N = 110$ K), indicating that magnetic order does not dominantly affect the HHG mechanism. The third harmonics slightly decreases by lowering temperature. For the fifth and higher harmonics, instead, HHG intensities exponentially increase down to about 200 K and then show a gradual saturation. The rate of increase of HHG signals is larger for higher harmonics. For comparison, we also measured HHG from the conventional narrow-gap semiconductor InAs (open squares in Figs. 3), which has a room-temperature gap energy (~0.3 eV) and carrier concentration (~10^{16} cm^{-3}) similar to those of Ca_2RuO_4 [37]. In contrast to Ca_2RuO_4, the HHG intensities that we measured for InAs are almost independent of temperature. Moreover, we confirmed that the effect of thermally activated carriers on the temperature dependence of the HHG yields is negligible by measuring HHG in La-doped Ca_2RuO_4 ($Ca_{2-x}La_xRuO_4$, x = 0.016) (see Figs. S4 and S5 in the Supplemental Material) [30,38]. These results imply that HHG in the Mott-insulating Ca_2RuO_4 is qualitatively different from those of conventional semiconductors.

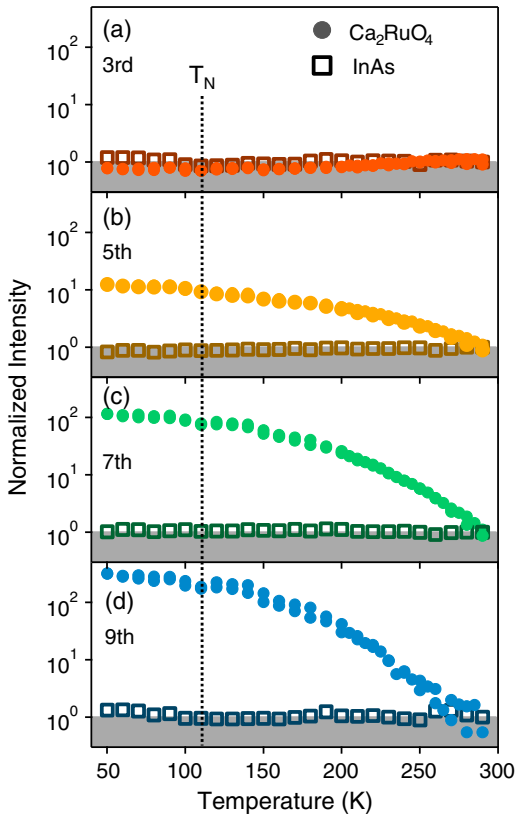

FIG. 3. Enhancement of HHG at low temperature. (a)–(d) Normalized (a) third, (b) fifth, (c) seventh, and (d) ninth harmonic intensity as a function of sample temperature with MIR intensity of 0.3 TW/cm^2 at $\theta = 45°$. Solid circles (open squares) indicate the HHG observed in Ca_2RuO_4 (InAs). Dashed lines at 110 K indicate the Néel temperature T_N.

We found that the observed enhancement in HHG yields at low temperature has a direct correlation with the optical gap energy 2Δ of Ca_2RuO_4. By using the temperature dependence $2\Delta(T)$ found in literature [29], we plot HHG intensities as a function of gap energy in Fig. 4(a). For the third-order harmonics, the intensity slightly decreases with increasing gap energy. The fifth and higher harmonic intensities, instead, increase with the gap energy. Moreover, HHG yields can be well described as exponential functions of $2\Delta(T)$. This clearly indicates a strong connection between the gap energy and HHG enhancement in Ca_2RuO_4. Surprisingly, our experimental results are contrary to what is expected from the carrier tunneling process, according to which an increase in gap energy suppresses carriers generated by the field tunneling process, diminishing the resulting HHG signal [39–41]. This suggests that increasing the gap energy enhances the nonlinearity of the system to an extent that overcomes the attenuation of tunneling carriers.

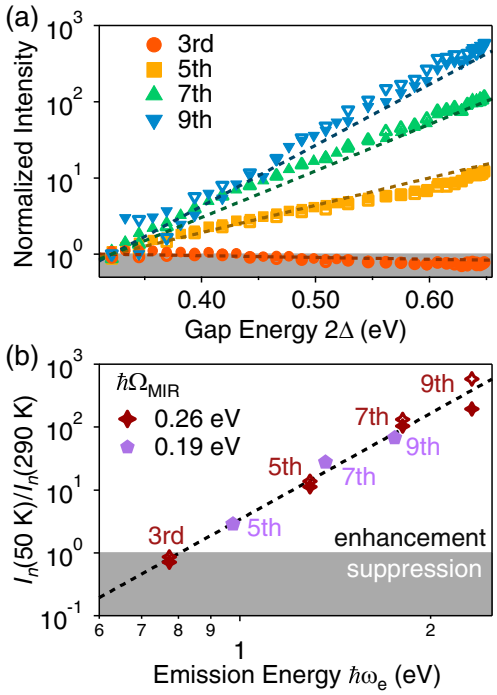

FIG. 4. Empirical scaling law of HHG enhancement in Ca_2RuO_4. (a) Normalized HHG intensity as a function of optical gap energy of Ca_2RuO_4 2Δ (gap energy *from literature* [29]). Orange circles, yellow squares, green triangles, and blue inverted triangles indicate the third, fifth, seventh, and ninth harmonics, respectively. Open (solid) symbols were measured with increasing (lowering) sample temperature. The dashed lines indicate the fitting curves by using Eq. (1) with $\hbar\Omega_{th} = 0.8$ eV and $2\Delta_{th} = 58$ meV. All the harmonic intensities are normalized by the values at 290 K. (b) Enhancement factor defined as the ratio of HHG intensity at 50 to 290 K $I_n(50\ \mathrm{K})/I_n(290\ \mathrm{K})$ as a function of emission energy. Brown diamonds and purple pentagons are measured with an MIR photon energy of 0.26 and 0.19 eV, respectively. Open (solid) symbols were measured with increasing (lowering) temperature. The dashed line indicates the fitting curve given by Eq. (1).

To obtain more information about the enhancement in HHG yields, we measured HHG with different incident MIR photon energies [30]. Figure 4(b) shows as a function of HHG emission energy $\hbar\omega_e$ the ratio of HHG intensity at 290 to that at 50 K, which we define as the enhancement factor. We compare the results obtained with two different incident MIR photon energies: $\hbar\Omega_{MIR} = 0.26$ (brown diamonds) and 0.19 eV (purple pentagons). Within the same harmonic order, the enhancement factor decreases as the incident photon energy decreases. Surprisingly, the enhancement factor follows a single power law [$\propto(\hbar\omega_e)^l$, $l \sim 5.6$] regardless of the incident photon energy. This indicates that the enhancement in HHG yields is not determined by the driving photon energy, but rather by the emission photon energy.

We propose an empirical scaling law that satisfies the characteristics of both the two experimental result in Figs. 4(a) and 4(b), where the nth order harmonic yield as a function of gap energy $2\Delta(T)$ and emission energy $\hbar\omega_e$ $(=n\hbar\Omega_{MIR})$ can be expressed by

$$I_n(T)/I_n(T_0) \approx \left(\frac{n\Omega_{MIR}}{\Omega_{th}}\right)^{\frac{\Delta(T)-\Delta(T_0)}{\Delta_{th}}}. \quad (1)$$

Here, $\hbar\Omega_{th}$ and $2\Delta_{th}$ are threshold values of the HHG emission energy and gap energy, respectively. We use Eq. (1) to fit the data in both Figs. 4(a) and 4(b) (dashed lines) and find good agreement with the experiment by using only two fit parameters $\hbar\Omega_{th} \sim 0.8$ eV and $2\Delta_{th} \sim 58$ meV. This empirical equation allows us to calculate the harmonic yields at temperature T when the HHG yields at a fixed temperature T_0 are known. Remarkably, Eq. (1) describes both the slight suppression of the third harmonic and the enhancement of the fifth and higher harmonics. Also, the fact that it is not the harmonic order but rather the HHG emission energy that determines the enhancement factor implies that the observed enhancements are regulated by the emission process. This simple, but rather extraordinary scaling law of HHG yields has never been reported in previous studies on HHG in solids.

In general, changes in electronic structures, such as band structure and transition dipole moment, can alter HHG yields [42–44]. When such changes occur, the optical conductivity spectrum, which is directly related to the material electronic structure, usually presents large modifications such as an increase in amplitude and the emergence of new peaks. However, there are no salient changes in Ca_2RuO_4 optical conductivity spectrum as a function of temperature, apart from a continuous temperature-driven gap opening [29,45]. In addition, possible temperature-induced changes in the electronic structure would result in strong changes of HHG yields as a function of MIR intensity [7]. This is because by changing the MIR

intensity, it is possible to span different momentum regions of the Brillouin zone, corresponding to about 2.4 to 6.0×10^{-9} m^{-1} for the intensities used in our experiment. However, we observe no salient changes in Figs. 2 in the studied range between 290 and 50 K. For these two reasons, we conclude that no significant changes occur both in Ca_2RuO_4 band structure and transition dipole moment, and thus the observed enhancement of the HHG yields in Ca_2RuO_4 must be attributed to a different cause.

A possible explanation within the single-electron approximation is that the gap opening upon lowering temperature directly enhances the HHG yields. To test this hypothesis, we performed a numerical calculation to understand whether changes in the band gap energy in a simple single particle model can lead to enhancement of HHG yields. The calculated HHG signals show nonmonotonic behavior as a function of the gap energy, and do not reproduce the experimental exponential enhancement (Figs. S8 and S9) [30]. This result suggests that the observed enhancement of HHG yields in Ca_2RuO_4 may be caused by other elements which are neglected in our simulation, such as electron-electron correlations or the dynamical modification of the electronic structure under driving field.

Although HHG in Mott insulators have been theoretically investigated by using the one-band Mott Hubbard model [16,17,46,47], previous calculations also do not capture the characteristics of our experimental results. In the calculations by Silva *et al.* and Orhtodoxou *et al.*, the emergence of broad emission spectrum above the gap energy associated with dynamical Mott breakdown has been predicted [16,46]. Although our experimental MIR electric field of 15 MV/cm is comparable to the one used in the calculations (10 MV/cm), we only observed peaks at harmonic emission energies $n\hbar\Omega_{\mathrm{MIR}}$ (where n is an odd number), without broadening of spectrum as shown in Fig. 1(c). Moreover, no scaling law of the HHG yields was found in previous simulations [16,17,46,47].

The fact that calculations cannot predict the scaling law in the HHG yields suggests that the simple one-band Mott Hubbard model is insufficient to describe nonlinear optical response in real Mott insulators. More refined theoretical investigation involving models with multiple degrees of freedom, which is neglected in the calculations, is needed to understand actual HHG process in Ca_2RuO_4. We note that in Ca_2RuO_4 degrees of freedom such as the on-site Coulomb repulsion, Hund coupling, crystal field splitting, and spin-orbit coupling are all in competition and contribute to determining the material ground state [48]. This competition is probably the key for the system nonlinearity. In addition, the dynamical modification of the electronic structure is one of the most essential characteristics in correlated electron systems under a driving field. In a system with multiple degrees of freedom, such changes are more pronounced and may lead to dramatic changes in the light-matter interaction such as the observed scaling law in the HHG yields.

In conclusion, we investigated the properties of HHG emission from Mott-insulating Ca_2RuO_4. HHG efficiencies whose orders are greater than the third show strong enhancement as the temperature is lowered. We found that the observed temperature dependence is strongly linked to temperature-driven changes of Ca_2RuO_4 gap energy, with an exponential enhancement in HHG yields as the gap energy increases. This enhancement does not occur in ordinary semiconductors, suggesting that electron-electron correlations and the competing of multiple degrees of freedom play an important role in the HHG mechanism in Ca_2RuO_4. The HHG enhancements observed in this work are well described by the empirical scaling law expressed by Eq. (1) that depends only on the material gap energy and HHG emission energy. This scaling law suggests that the HHG process in Ca_2RuO_4 underlies a physics peculiar to strongly correlated systems. Further theoretical and experimental studies, focusing specifically on the nonlinear optical response of strongly correlated materials, may help to elucidate the possible universality of the observed scaling law. In addition, further probing the electronic structure change with MIR drive may allow direct access to HHG processes in strongly correlated materials, but it is beyond the scope of this Letter. These undertakings will lead to a further understanding of strongly correlated materials, possibly enabling us to control many-body structures on an ultrafast timescale and ultimately to design novel functional materials.

The authors are thankful to Hideki Narita for characterizing La-doped Ca_2RuO_4 samples. K. U. and K. T. are thankful to Yuta Murakami and Kazuaki Takasan for fruitful discussions. This work was supported by Grant-in-Aid for Scientific Research (S) (Grants No. JP21H05017, No. JP17H06124 and No. JP17H06136), JST ACCEL Grant (No. JPMJMI17F2), and the JSPS Core-to-Core Program (No. JPJSCCA20170002). K. U. is thankful for a Grant-in-Aid for Young Scientists (Grant No. 19K14632). G. M. acknowledges the support from the Dutch Research Council (NWO) through Rubicon Grant No. 019.183EN.031.

*Corresponding author.
uchida.kento.4z@kyoto-u.ac.jp
†Corresponding author.
kochan@scphys.kyoto-u.ac.jp

[1] D. Fausti, R. I. Tobey, N. Dean, S. Kaiser, A. Dienst, M. C. Hoffmann, S. Pyon, T. Takayama, H. Takagi, and A. Cavalleri, Light-induced superconductivity in a stripe-ordered cuprate, Science **331**, 189 (2011).
[2] X. Li, T. Qiu, J. Zhang, E. Baldini, J. Lu, A. M. Rappe, and K. A. Nelson, Terahertz field-induced ferroelectricity in quantum paraelectric $SrTiO_3$, Science **364**, 1079 (2019).

[3] T. Kampfrath, K. Tanaka, and K. A. Nelson, Resonant and nonresonant control over matter and light by intense terahertz transients, Nat. Photonics **7**, 680 (2013).

[4] C. Giannetti, M. Capone, D. Fausti, M. Fabrizio, F. Parmigiani, and D. Mihailovic, Ultrafast optical spectroscopy of strongly correlated materials and high-temperature superconductors: A non-equilibrium approach, Adv. Phys. **65**, 58 (2016).

[5] S. Ghimire, A. D. DiChiara, E. Sistrunk, P. Agostini, L. F. DiMauro, and D. A. Reis, Observation of high-order harmonic generation in a bulk crystal, Nat. Phys. **7**, 138 (2011).

[6] O. Schubert, M. Hohenleutner, F. Langer, B. Urbanek, C. Lange, U. Huttener, D. Golde, T. Meier, M. Kira, S. W. Koch, and R. Huber, Sub-cycle control of terahertz high-harmonic generation by dynamical Bloch oscillations, Nat. Photonics **8**, 119 (2014).

[7] T. T. Luu, M. Garg, S. Yu. Kruchinin, A. Moulet, M. Th. Hassan, and E. Goulielmakis, Extreme ultraviolet high-harmonic spectroscopy of solids, Nature (London) **521**, 498 (2015).

[8] G. Vampa, T. J. Hammond, N. Thiré, B. E. Schmidt, F. Légaré, C. R. McDonald, T. Brabec, D. D. Klug, and P. B. Corkum, All-Optical Reconstruction of Crystal Band Structure, Phys. Rev. Lett. **115**, 193603 (2015).

[9] Y. S. You, D. A. Reis, and S. Ghimire, Anisotropic high-harmonic generation in bulk crystals, Nat. Phys. **13**, 345 (2017).

[10] N. Yoshikawa, T. Tamaya, and K. Tanaka, High-harmonic generation in graphene enhanced by elliptically polarized light excitation, Science **356**, 736 (2017).

[11] T. T. Luu and H. J. Wörner, Measurement of the Berry curvature of solids using high-harmonic spectroscopy, Nat. Commun. **9**, 916 (2018).

[12] K. Kaneshima, Y. Shinohara, K. Takeuchi, N. Ishii, K. Imasaka, T. Kaji, S. Ashihara, K. L. Ishikawa, and J. Itatani, Polarization-Resolved Study of High Harmonics from Bulk Semiconductors, Phys. Rev. Lett. **120**, 243903 (2018).

[13] S. Ghimire and D. A. Reis, High-harmonic generation from solids, Nat. Phys. **15**, 10 (2019).

[14] H. Lakhotia, H. Y. Kim, M. Zhan, S. Hu, S. Meng, and E. Goulielmakis, Laser picoscopy of valence electrons in solids, Nature (London) **583**, 55 (2020).

[15] K. Uchida, V. Pareek, K. Nagai, K. M. Dani, and K. Tanaka, Visualization of two-dimensional transition dipole moment texture in momentum space using high-harmonic generation spectroscopy, Phys. Rev. B **103**, L161406 (2021).

[16] R. E. F. Silva, I. V. Blinov, A. N. Rubtsov, O. Smirnova, and M. Ivanov, High-harmonic spectroscopy of ultrafast many-body dynamics in strongly correlated systems, Nat. Photonics **12**, 266 (2018).

[17] Y. Murakami, M. Eckstein, and P. Werner, High-Harmonic Generation in Mott Insulators, Phys. Rev. Lett. **121**, 057405 (2018).

[18] N. Tancogne-Dejean, M. A. Sentef, and A. Rubio, Ultrafast Modification of Hubbard U in a Strongly Correlated Material: *Ab initio* High-Harmonic Generation in NiO, Phys. Rev. Lett. **121**, 097402 (2018).

[19] S. Imai, A. Ono, and S. Ishihara, High Harmonic Generation in a Correlated Electron System, Phys. Rev. Lett. **124**, 157404 (2020).

[20] Y. Michishita and R. Peter, Effects of renormalization and non-Hermiticity on nonlinear responses in strongly correlated electron systems, Phys. Rev. B **103**, 195133 (2021).

[21] M. R. Bionta, E. Haddad, A. Leblanc, V. Gruson, P. Lassonde, H. Ibrahim, J. Chaillou, N. Emond, M. R. Otto, B. J. Siwick, M. Chaker, and F. Légaré, Tracking ultrafast solid-state dynamics using high harmonic spectroscopy, Phys. Rev. Research **3**, 023250 (2021).

[22] O. Gränäs *et al.*, Ultrafast modification of the electronic structure of a correlated insulator, arXiv:2008.11115.

[23] S. Nakatsuji, S. Ikeda, and Y. Maeno, Ca_2RuO_4: New Mott insulators of layered ruthenate, J. Phys. Soc. Jpn. **66**, 1868 (1997).

[24] G. Cao, S. McCall, M. Shephard, J. E. Crow, and R. P. Guertin, Thermal, magnetic, and transport properties of single-crystal $Sr_{1-x}Ca_xRuO_3 (0 < \sim x < \sim 1.0)$, Phys. Rev. B **56**, 321 (1997).

[25] C. S. Alexander, G. Cao, V. Dobrosavljevic, S. McCall, J. E. Crow, E. Lochner, and R. P. Guertin, Destruction of the Mott insulating ground state of Ca_2RuO_4 by a structural transition, Phys. Rev. B **60**, R8422 (1999).

[26] S. Nakatsuji and Y. Maeno, Quasi-Two-Dimensional Mott Transition system $Ca_{2-x}Sr_xRuO_4$, Phys. Rev. Lett. **84**, 2666 (2000).

[27] F. Nakamura, T. Goko, M. Ito, T. Fujita, S. Nakatsuji, H. Fukazawa, Y. Maeno, P. Alireza, D. Forsythe, and S. R. Julian, From Mott insulator to ferromagnetic metal: A pressure study of Ca_2RuO_4, Phys. Rev. B **65**, 220402(R) (2002).

[28] F. Nakamura, M. Sakaki, Y. Yamanaka, S. Tamaru, T. Suzuki, and Y. Maeno, Electric-field-induced metal maintained by current of the Mott insulator Ca_2RuO_4, Sci. Rep. **3**, 2536 (2013).

[29] J. H. Jung, Z. Fang, J. P. He, Y. Kaneko, Y. Okimoto, and T. Tokura, Change of Electronic Structure in Ca_2RuO_4 Induced by Orbital Ordering, Phys. Rev. Lett. **91**, 056403 (2003).

[30] See Supplemental Material at http://link.aps.org/supplemental/10.1103/PhysRevLett.128.127401 for additional details, which includes Refs [31–33].

[31] A. J. Uzan *et al.*, Attosecond spectral singularities in solid-state high-harmonic generation, Nat. Photonics **14**, 183 (2020).

[32] G. Vampa, C. R. McDonald, G. Orlando, P. B. Corkum, and T. Brabec, Semiclassical analysis of high harmonic generation in bulk crystals, Phys. Rev. B **91**, 064302 (2015).

[33] Y. P. Varshni, Temperature dependence of the energy gap in semiconductors, Physica **34**, 149 (1967).

[34] G. Vampa, Y. S. You, H. Liu, S. Ghimire, and D. A. Reis, Observation of backward high-harmonic emission from solids, Opt. Express **26**, 12210 (2018).

[35] P. Xia, C. Kim, F. Lu, T. Kanai, H. Akiyama, J. Itatani, and N. Ishii, Nonlinear propagation effects in high harmonic generation in reflection and transmission from gallium arsenide, Opt. Express **26**, 29393 (2018).

[36] I. Floss, C. Lemell, G. Wachter, V. Smejkal, S. A. Sato, X. M. Tong, K. Yabana, and J. Burgdörfer, *Ab initio* multiscale simulation of high-order harmonic generation in solids, Phys. Rev. A **97**, 011401(R) (2018).

[37] R. Okazaki, Y. Nishina, Y. Yasui, and F. Nakamura, Current-induced gap suppression in the Mott insulator Ca_2RuO_4, J. Phys. Soc. Jpn. **82**, 103702 (2013).

[38] G. Cao, S. McCall, V. Dobrosavljevic, C. S. Alexander, J. E. Crow, and R. P. Guertin, Ground-state instability of the Mott insulator Ca_2RuO_4: Impact of slight La doping on the metal-insulator transition and magnetic ordering, Phys. Rev. B **61**, R5053 (2000).

[39] T. Oka, R. Arita, and H. Aoki, Breakdown of a Mott Insulator: A Nonadiabatic Tunneling Mechanism, Phys. Rev. Lett. **91**, 066406 (2003).

[40] T. Oka and H. Aoki, Ground-State Decay Rate for the Zener Breakdown in Band and Mott Insulators, Phys. Rev. Lett. **95**, 137601 (2005).

[41] H. Yamakawa, T. Miyamoto, T. Morimoto, T. Terashige, H. Yada, N. Kida, M. Suda, H. M. Yamamoto, R. Kato, K. Miyagawa, K. Kanoda, and H. Okamoto, Mott transition by an impulsive dielectric breakdown, Nat. Mater. **16**, 1100 (2017).

[42] N. Yoshikawa, K. Nagai, K. Uchida, Y. Takaguchi, S. Sasaki, Y. Miyata, and K. Tanaka, Interband resonant high-harmonic generation by valley polarized electron–hole pairs, Nat. Commun. **10**, 3709 (2019).

[43] C. Yu, X. Zhang, S. Jiang, X. Cao, G. Yuan, T. Wu, L. Bai, and R. Lu, Dependence of higher-order-harmonic generation on dipole moment in SiO_2 crystals, Phys. Rev. A **94**, 013846 (2016).

[44] S. Jiang, J. Chen, H. Wei, C. Yu, R. Lu, and C. D. Lin, Role of the Transition Dipole Amplitude and Phase on the Generation of Odd and Even High-Order Harmonics in Crystals, Phys. Rev. Lett. **120**, 253201 (2018).

[45] J. H. Jung, Raman scattering and optical absorption studies of an orbital ordered Ca_2RuO_4, Solid State Commun. **133**, 103 (2005).

[46] C. Orhtodoxou, A. Zaïr, and G. H. Booth, High harmonic generation in two-dimensional Mott insulators, Quantum Mater. **6**, 76 (2021).

[47] Y. Murakami, S. Takayoshi, A. Koga, and P. Werner, High-harmonic generation in one-dimensional Mott insulators, Phys. Rev. B **103**, 035110 (2021).

[48] L. Das *et al.*, Spin-Orbital Excitations in Ca_2RuO_4 Revealed by Resonant Inelastic X-Ray Scattering, Phys. Rev. X **8**, 011048 2018).